JVI Journals.ASM.org

Genetic Inactivation of COPI Coatomer Separately Inhibits Vesicular Stomatitis Virus Entry and Gene Expression

David K. Cureton,* Rebeca Burdeinick-Kerr, and Sean P. J. Whelan

Department of Microbiology and Immunobiology, Harvard Medical School, Boston, Massachusetts, USA

Viruses coopt cellular membrane transport to invade cells, establish intracellular sites of replication, and release progeny virions. Recent genome-wide RNA interference (RNAi) screens revealed that genetically divergent viruses require biosynthetic membrane transport by the COPI coatomer complex for efficient replication. Here we found that disrupting COPI function by RNAi inhibited an early stage of vesicular stomatitis virus (VSV) replication. To dissect which replication stage(s) was affected by coatomer inactivation, we used visual and biochemical assays to independently measure the efficiency of viral entry and gene expression in hamster (ldlF) cells depleted of the temperature-sensitive ε-COP subunit. We show that ε-COP depletion for 12 h caused a primary block to virus internalization and a secondary defect in viral gene expression. Using brefeldin A (BFA), a chemical inhibitor of COPI function, we demonstrate that short-term (1-h) BFA treatments inhibit VSV gene expression, while only long-term (12-h) treatments block virus entry. We conclude that prolonged coatomer inactivation perturbs cellular endocytic transport and thereby indirectly impairs VSV entry. Our results offer an explanation of why COPI coatomer is frequently identified in screens for cellular factors that support cell invasion by microbial pathogens.

Vesicular stomatitis virus (VSV) is the prototype member of the *Rhabdoviridae* family. In cell culture, VSV can replicate in a wide variety of cell types, including nearly all mammalian cells as well as cells from insects (47), nematodes (55, 69), and yeast (40). This capacity to infect cells from model genetic organisms, along with its genetic tractability, makes VSV an ideal model for probing virus-host cell interactions. VSV virions are bullet shaped and measure ~75 by 200 nm (15, 49). Each virion contains a condensed, helical ribonucleoprotein (RNP) core that consists of a single strand of viral genomic RNA encased within a protein shell of nucleocapsid (N) protein, together with the phosphoprotein (P) and large (L) polymerase protein that constitute the viral RNA-dependent RNA polymerase (39, 49). The helical packing of the RNP is stabilized by matrix (M) proteins, and the M-RNP complex is tightly enveloped within a bilayer of lipids (48, 49). Protruding from this lipid bilayer are ~400 homotrimers of the viral attachment and fusion glycoprotein (G) (49, 61).

The VSV replication cycle can be summarized as follows. Virus particles attach to target cells through low-affinity, electrostatic interactions between G proteins and charged moieties on the cell surface (4, 10). Cells internalize the attached particles by clathrin-dependent endocytosis (14, 15, 29, 41, 58), and this uptake mechanism delivers the particles to early endosomes (EEs). Endosome acidification to a pH of ≤6.3 triggers conformational changes in the G proteins that in turn force fusion between the viral and cellular membranes and release of the viral RNP into the host cell cytosol (67). The endosomal location(s) of VSV membrane fusion and RNP release is currently uncertain, with available evidence supporting membrane penetration of EEs (29, 38, 57) as well as downstream endosomal compartments (32). During or shortly after RNP release, M protein dissociates from the RNP to facilitate mRNA synthesis in the cell cytoplasm (44, 53). Translation of the viral mRNA is essential to support viral genome replication, since it provides a source of N protein necessary to encapsidate the genomic and antigenomic RNA. Newly synthesized RNPs are then assembled into progeny particles at the cellular plasma membrane, where M proteins drive RNP budding through the G-containing lipid bilayer (39).

Genome-wide RNA interference (RNAi) screens have implicated numerous cellular factors as important for the replication of obligate intracellular pathogens. One cellular factor that has been identified in a majority of these screens is COPI coatomer (1, 2, 8, 12, 13, 17, 18, 24, 31, 35, 45, 50, 51, 60). Coatomer is comprised of 7 subunits (α-, β-, β′-, δ-, ε-, γ-, and ζ-COP) that are recruited as subcomplexes from the cell cytosol to Golgi membranes by the GTPase ADP ribosylation factor 1 (Arf1) (7). Assembly of these subcomplexes into a coat-like structure promotes the budding of membrane-bound vesicles that transport cargos within the cellular biosynthetic pathway (6). In addition to this well-characterized function, COPI has also been attributed a role in endocytic cargo transport from EEs to late endosomes (LEs). *In vitro*, coatomer subunits bind endosomal membranes and facilitate cargo delivery from isolated EEs to LEs (3, 21, 22, 68). In cells, COPI subunits also associate with endosomes, yet the precise function of coatomer in this context remains uncertain (68).

The consequences of coatomer inactivation for cellular membrane traffic have been extensively investigated. In cells treated with a chemical inhibitor of coatomer function, brefeldin A (BFA), the Golgi apparatus merges with the endoplasmic reticulum (ER) and endocytic compartments, which arrests protein secretion and decreases endocytic cargo transport to lysosomes (26, 36, 37, 46). Depletion of the temperature-sensitive ε-COP subunit

Received 27 July 2011 **Accepted** 26 October 2011

Published ahead of print 9 November 2011

Address correspondence to Sean P. J. Whelan, swhelan@hms.harvard.edu, or David K. Cureton, cureton@idi.harvard.edu.

* Present address: Department of Cell Biology, Harvard Medical School, and Immune Disease Institute, Boston, MA 02115.

doi:10.1128/JVI.05810-11

in Chinese hamster ovary (ldlF) cells also blocks protein secretion, induces low-density lipoprotein receptor degradation, and decreases the uptake and delivery of certain endocytic cargos to lysosomes (16, 23, 27). In the context of viral infections, BFA inhibits stages of viral replication that rely upon cellular biosynthetic transport (19, 28, 63, 64), and ε-COP depletion in ldlF cells blocks early stages of Semliki forest virus (SFV) and VSV replication (16). However, in most virus systems, it is still unclear which steps of viral replication directly require coatomer function.

In this study, we examined how COPI inactivation impairs VSV infection. We employed genetic and chemical methods to inhibit COPI function and a panel of new assays to quantify the effects of these perturbations on steps of virus entry and gene expression. We found that genetic depletion of ε-COP inhibited VSV internalization and viral gene expression. However, the effect of ε-COP depletion on virus internalization could be reproduced only by long-term treatment of cells with BFA. We conclude that COPI function is critical for multiple stages of VSV replication. Moreover, our findings underscore that long-term coatomer inactivation indirectly perturbs endocytic transport, which may contribute to the inhibitory effect of small interfering RNA (siRNA)-mediated COPI depletion on cell invasion by other microbes.

MATERIALS AND METHODS

Cells and reagents. Baby hamster kidney BsrT7 cells (9) and human cervix adenocarcinoma HeLa S3 cells (ATCC clone CCL-2.2) were maintained at 37°C and 5% CO_2 in Dulbecco's modified Eagle's medium (Invitrogen Corporation, Carlsbad, CA) containing 10% fetal bovine serum (FBS) (Tissue Culture Biologicals, Tulare, CA). Chinese hamster ovary (CHO) and ldlF cells (gift of Monty Krieger, MIT) were maintained at 34°C and 5% CO_2 in Ham's F-12 nutrient medium (Invitrogen) supplemented with 5% FBS (Tissue Culture Biologicals). Puromycin, cycloheximide (CHX), brefeldin A (BFA), bafilomycin A1 (BAF), and ammonium chloride were purchased from Sigma-Aldrich (St. Louis, MO).

Recombinant viruses. The infectious cDNA clones of VSV (65), VSV-enhanced green fluorescent protein (VSV-eGFP) (11), and VSV-eGFP-P (55) were previously reported. The VSV cDNA clone encoding an amino-terminal fusion of *Renilla* luciferase to the phosphoprotein (VSV REN-P) was constructed as for VSV-eGFP-P (55) except that the gene for *Renilla* luciferase was substituted for that of eGFP. VSV REN-P was recovered from plasmid DNA using standard reverse genetics techniques (65). Working stocks were prepared from plaque-isolated virus, and sequencing of the entire viral genome confirmed that no undesired mutations were introduced during virus recovery and amplification. To prepare purified virus stocks, concentrated virions were banded on a linear 15 to 45% sucrose gradient in NTE (10 mM Tris [pH 7.4], 100 mM NaCl, 1 mM EDTA), and isolated particles were stored in NTE at −80°C. Virus titers were measured by plaque assay on Vero cells. To examine the protein composition of purified virions, 5 μg of total viral protein was analyzed by electrophoresis through a low-bis 10% SDS-polyacrylamide gel, and the proteins were visualized by Coomassie blue staining.

RNA interference screen. SMART pools (Thermo Fisher Scientific, Dharmacon, Chicago, IL) comprised of four duplexes targeting a single human mRNA transcript were individually arrayed into wells of black, clear-bottom 384-well plates (Costar 3712; Corning, Lowell, MA) containing a 1:100 dilution of Lipofectamine 2000 (Invitrogen) in Opti-MEM (Invitrogen). Duplexes and lipids were incubated for 20 min at room temperature (RT) and mixed with HeLa cells to yield final concentrations of 5×10^4 cells ml^{-1} and 25 nM siRNA. Plates were inoculated with 1,250 HeLa cells per well, and cells were centrifuged for 5 min at 700 × *g*. At 48 h posttransfection, the cells (~5,000 per well) were inoculated with 25,000 infectious particles of VSV-eGFP (according to the titer on Vero cells). This virus dose reproducibly infected ~50% of untransfected HeLa cells. Cells were fixed 7 h later with 2% formaldehyde in phosphate-buffered saline (PBS). Nuclei were counterstained with 4 μg ml^{-1} Hoechst nuclear dye (33342; Invitrogen) for 10 min at RT, and unincorporated dye was removed by washing once with PBS. Images were acquired from each well using a cellWoRX high-content cell analysis system (Applied Precision Inc., Issaquah, WA). The total number of cells and percentage of eGFP-positive cells in each image were scored using MetaXpress software (Molecular Devices, Dowingtown, PA).

For each gene, 2 wells in separate plates were transfected with siRNA and then infected with virus. Each well plate contained 1 well each of the following controls: (i) buffer control (BC) with no transfection reagent or siRNA, (ii) cells treated with siGENOME nontargeting (NT) siRNA 2 (Dharmacon catalog no. D-001210-02) (negative control for transfection toxicity), and (iii) cells treated with siGENOME SMARTpool eIF1AX (Dharmacon catalog no. M-011262) targeting eIF1-alpha (positive control, reduces the percentage of infected cells by 50%). To compare the relative effects of each siRNA pool on virus infection, the percentage of infected cells in each test or control sample was divided by the percentage of infected cells in the BC sample from the same plate. The calculated values for test samples from the 2 separate plates were then averaged, multiplied by 100, and plotted as mean ± standard deviation (SD). The calculated values for the nontargeting and eIF1-alpha control samples were averaged across all 5 plates that contained the COPI test samples, multiplied by 100, and plotted as mean ± SD. A secondary screen was conducted in which five coatomer subunits were targeted for siRNA-mediated depletion. All aspects of the secondary screen were performed as for the primary screen except that cells were separately transfected with 25 nM of the four individual siRNAs (see Table 1 for siRNA catalog numbers) that comprised the SMARTpools used in the primary screen.

Western blotting. CHO and ldlF cells were harvested, pelleted by centrifugation, and lysed in total cell lysis buffer (25 mM HEPES, 1% Triton X-100, 10% glycerol, 300 mM NaCl, 1.5 mM $MgCl_2$, 2 mM EDTA, 2 mM EGTA, 1 mM dithiothreitol [DTT], 1 mM phenylmethylsulfonyl fluoride [PMSF], Complete protease inhibitor cocktail [Roche Applied Biosciences; Indianapolis, IN]). Samples were centrifuged for 15 min. at 15,000 × *g* and 4°C, and 10 μg of total protein was analyzed on a 10% SDS-polyacrylamide gel. Proteins were transferred to a nitrocellulose membrane (GE Healthcare, United Kingdom) and blocked in Tris-buffered saline (20 mM Tris-HCl [pH 7.4], 150 mM NaCl) containing 0.05% Tween 20 (TBST) and 5% (wt/vol) milk for 1 h at room temperature (RT). Membranes were incubated with rabbit anti-ε-COP (gift of Monty Krieger) in TBST containing 1% milk for 1 h at RT. Membranes were washed 3 times in TBST for a total of 30 min, and the primary antibodies were detected using goat anti-rabbit–horseradish peroxidase (HRP) antibodies (Sigma-Aldrich) as described above. Membranes were washed, and HRP was detected by enhanced chemiluminescence (Thermo Fisher Scientific, Pierce, Rockford, IL) according to the manufacturer's instructions.

Enzymatic assays for VSV attachment and RNP release. To quantify VSV attachment, confluent CHO or ldlF cells in a 96-well plate were rapidly cooled in an ice water bath and inoculated with 7.5×10^6 PFU of untreated VSV REN-P (multiplicity of infection [MOI], 250) or virus preincubated with a neutralizing monoclonal antibody directed against G protein (IE-2; a kind gift of Isabella Novella) (62). Cells and virus were incubated for 1 h at 4°C, and unbound virus was removed by washing. The quantity of attached virus particles was measured by lysis of the virus-cell complexes in the presence of the *Renilla* luciferase substrate (*Renilla* luciferase assay system; Promega, Madison, WI). To detect RNP release by VSV REN-P, CHO cells were inoculated with 60 μM EnduRen (Promega) in Ham's medium containing 2% FBS. After incubation for 30 min at the indicated temperature, puromycin was added to a final concentration of 50 μg ml^{-1}, and cells were incubated for 1 additional hour. Treated cells were inoculated with 7.5×10^5 PFU (MOI, 25) of untreated VSV REN-P per well or the same quantity of virus preincubated with neutralizing

antibody IE-2 (see above), and luminescence was quantified at the indicated times postinoculation (p.i.) using a Microbeta TriLux scintillation counter (Perkin-Elmer, Waltham, MA). In all experiments, we ensured that the measured luminescence values were within the linear detection range of the instrument.

Measurements of VSV REN-P attachment and RNP release were conducted using triplicate samples for each experimental condition. Data from a single experimental setting are reported as the mean ± SD from the triplicate samples. If data are derived from more than one experiment (see figure legends), the plotted values are an average ± SD of the triplicate means from each experiment.

RNP purification and cell transfection. RNPs were isolated from purified VSV REN-P virions as described before (59). The protein composition of purified RNPs was analyzed by SDS-PAGE analysis, which showed that the RNPs consisted of N, P, and L proteins but lacked detectable M and G (see Fig. 2C). We also confirmed by plaque assay that the purified RNPs did not contain infectious virus particles. To quantify gene expression from transfected RNPs or plasmid DNA encoding *Renilla* luciferase (phRL-CMV; Promega), CHO cells in a 96-well plate (~20,000 cells per well) were transfected with 9 ng of total RNP protein or 40 ng of plasmid DNA using Lipofectamine 2000 (Invitrogen) according to the manufacturer's instructions, except that the amount of transfection reagent was reduced to 0.5 μl per well. Samples were maintained at the indicated temperature during the transfection reaction, and luminescence emitted from the transfected cells was quantified at 5 h posttransfection as described for the VSV REN-P attachment experiments.

UV irradiation of virus particles. Purified VSV REN-P particles were diluted to 1×10^6 PFU μl^{-1} in NTE (pH 7.4), and the diluted virions were exposed to UV light at a dose of 41 ergs mm^{-2} s^{-1} for the indicated length of time using a UV germicidal lamp in a SterilGARD III Advance biosafety hood (The Baker Company, Sanford, ME).

Fluorescent dye conjugation to VSV particles. Alexa Fluor 647 succinimidyl ester dye molecules (Invitrogen) were conjugated to G proteins on purified VSV and VSV-eGFP-P particles as previously described (14). Plaque assays of labeled particles showed that dye conjugation did not reduce virus infectivity.

Visual assays for steps of VSV entry. (i) Internalization. Cells grown on 12-mm coverslips (no. 1.5; Electron Microscopy Sciences, Hatfield, PA) were incubated with Alexa 647 VSV (MOI, 500) for the indicated time intervals, and samples were fixed in 2% paraformaldehyde (PFA) for 15 min at RT. This dose of virus permitted unambiguous counting of single particles and exclusion of endosomal virus signals that corresponded to more than one particle. To visualize the cellular plasma membrane, samples were incubated with 1 μg ml^{-1} Alexa Fluor 594 wheat germ agglutinin (WGA) (Invitrogen) for 20 min at RT. External virus particles were fluorescently labeled by incubating samples with IE-2, a monoclonal antibody specific for VSV G (62), followed by Alexa 488 (VSV)- and Alexa 594 (VSV-eGFP-P)-conjugated goat anti-mouse secondary antibodies (Invitrogen). All antibody incubation steps were conducted for 30 min at RT in the absence of detergent to exclusively label surface-bound virions. Transferrin (Tf) uptake was performed by incubating cells with 40 μg ml^{-1} of Alexa Fluor 488 human Tf (Invitrogen) in Ham's F-12 medium lacking serum. Surface-bound Tf was removed by washing cells for 2 min at 37°C in pH 4.6 citrate buffer (25 mM citric acid, 25 mM sodium citrate, 280 mM sucrose, and 0.01 mM deferoxamine mesylate), followed by two rinses in PBS (pH 7.4) (20). Acid-washed cells were then fixed and incubated with WGA as described above. Coverslips were mounted onto glass coverslips using ProLong Gold antifade reagent (Invitrogen).

(ii) RNP release. Cells grown on 12-mm coverslips (no. 1.5; Electron Microscopy Sciences) were incubated with Alexa 647-labeled VSV-eGFP-P (MOI, 500) for the indicated time intervals, and samples were fixed with 4% PFA for 15 min at RT. Extracellular virions were detected as in the virus internalization assay, except that goat anti-mouse secondary antibodies labeled with Alexa 594 (Invitrogen) were used. Viral N protein was detected in the presence of detergent using the monoclonal antibody 10G4 (34) and goat anti-mouse secondary antibodies labeled with Alexa 594 (Invitrogen). Coverslips were mounted onto glass slides using 0.1 M phosphate buffer, 90% (vol/vol) glycerol, and 3% 1,4-diazobicyclo-[2.2.2]-octane (DABCO) (Sigma-Aldrich) and sealed with nail polish. Samples were imaged prior to dehydration of the mounting buffer.

Image acquisition and processing. VSV and Tf internalization samples were analyzed by acquiring images spaced at 0.5-μm intervals encompassing the entire cell volume, using a spinning confocal microscope (15) controlled by Slidebook 4.2 (Intelligent Imaging Innovations, Denver, CO). Image planes were viewed using Slidebook, and the number of virus particles per cell was manually counted. Figure images were prepared using Slidebook.

RESULTS

COPI function is required for VSV replication. We genetically perturbed COPI function and quantified the effects on VSV replication. We transfected HeLa cells with siRNA pools targeting each coatomer subunit and inoculated the cells 48 h later with a recombinant VSV encoding eGFP (VSV-eGFP). At 7 h postinoculation (p.i.), we acquired images of the cell populations and used automated image analysis to quantify the number of total and eGFP-positive cells in each sample. RNAs targeting 7 of 9 COPI subunits reduced the percentage of eGFP-positive cells by 50 to 90% compared to control samples (Fig. 1A and B), while only RNAs targeting α-COP significantly reduced cell viability (Fig. 1B). Results of an independent screen confirmed that each siRNA pool contained at least one individual duplex that recapitulated the original screen results (Table 1). Since eGFP expression at 7 h p.i. does not depend on virus assembly or release, we conclude that COPI function is critical for a step(s) of VSV replication that precedes progeny virion assembly.

To independently corroborate the siRNA results, we used a Chinese hamster ovary (CHO) cell line (ldlF) with a temperature-sensitive lesion in ε-COP (27). This cell line has the added advantage of allowing us to examine how a more rapid loss of COPI function affects VSV replication. As expected, incubation of ldlF cells at the nonpermissive temperature (40°C) depleted ε-COP within 12 h (Fig. 2A). We quantified the efficiency of VSV-eGFP infection in CHO and ldlF cells by flow cytometry. VSV-eGFP infected and expressed eGFP to comparable levels in ldlF cells incubated at 34°C (Fig. 2B). In contrast, preincubation of ldlF cells at 40°C decreased cell infection by ~40% and reduced the mean fluorescence intensity of the infected cell population by 85% relative to that in wild-type (wt) cell samples (Fig. 2B). These data confirm our results from the HeLa cell screen and show that COPI function is critical for an early stage(s) of the viral replication cycle.

To bypass virus entry and quantify the effect of ε-COP depletion on gene expression alone, we transfected purified RNPs (Fig. 2C) into CHO cells and measured the luminescence generated from a virally encoded fusion of *Renilla* luciferase to VSV P (see Fig. 3 for details). The endpoint luminescence in RNP-transfected cells scaled in proportion to the amount of input RNPs, showing that this approach quantitatively measures viral gene expression separately from virus entry (Fig. 2C). Inactivation of coatomer function by incubation of ldlF cells for 12 h at the nonpermissive temperature decreased viral gene expression 2-fold relative to that in wt cells, while gene expression was equally efficient in CHO and ldlF cells that were maintained at 34°C (Fig. 2D). Coatomer inactivation did not alter the capacity of ldlF cells to express *Renilla* luciferase from transfected plasmid DNA, indicating that the cells

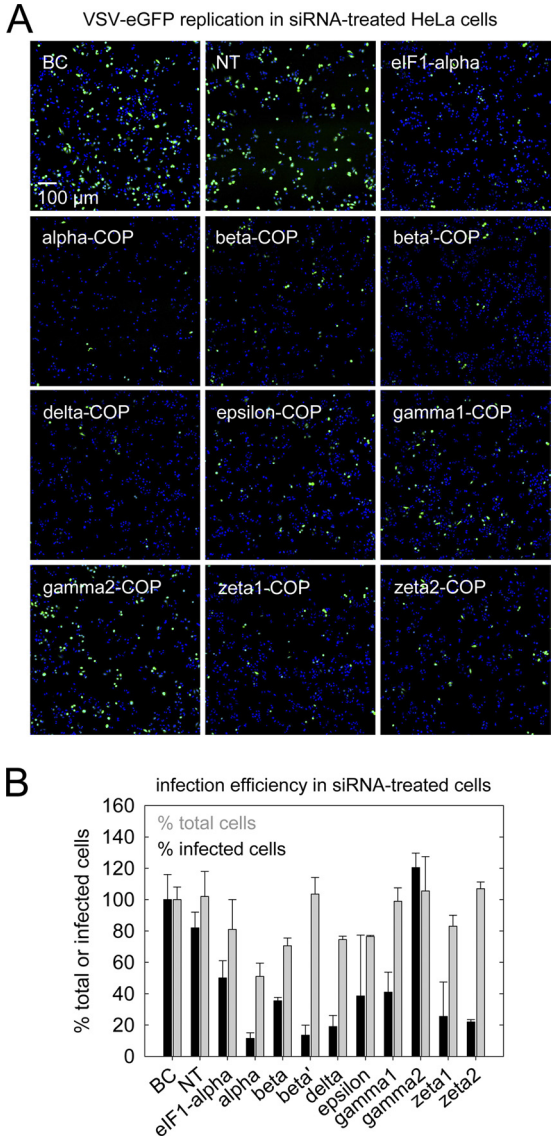

FIG 1 siRNAs targeting COPI coatomer subunits inhibit VSV replication. (A) Images of VSV replication in siRNA-treated cells. HeLa cells were treated with siRNAs and infected with VSV-eGFP as described in Materials and Methods. Images of cells treated with the indicated siRNAs were acquired using an automated epifluorescence microscope, and overlays of the nuclear Hoechst stain (blue) and eGFP (green) channels are shown. Knockdown of eIF1-alpha reproducibly decreased the percentage of infected cells by ~50% and served as a positive control in the screen. BC, no-siRNA buffer control. NT, nontargeting siRNA. (B) Effect of siRNAs targeting subunits of the COPI coatomer complex on VSV infection and cell viability. Automated image analysis was used to count the total number of nuclei and eGFP-positive cells in each sample. The plotted values were calculated as described in Materials and Methods and expressed as a percentage of the value for the BC samples.

were competent for transfection and protein synthesis (Fig. 2D). These results show that coatomer inactivation inhibits VSV gene expression. However, this moderate effect on gene expression does not account for the overall decrease in eGFP signal observed in the flow cytometry assay, suggesting that ε-COP depletion perturbs virus entry.

A virion-based enzymatic reporter of virus particle number. To test the hypothesis that ε-COP depletion inhibits VSV entry, we developed quantitative, enzyme-based assays that measure viral attachment and cytosolic RNP translocation independent of downstream gene expression. We generated a recombinant virus (VSV REN-P) that encodes an amino-terminal fusion of *Renilla* luciferase to the VSV P (Fig. 3). VSV REN-P replicates with kinetics similar to those of wt VSV (Fig. 3A) but has a smaller plaque size and releases fewer infectious particles (Fig. 3A). An analysis of virion protein composition showed that purified VSV REN-P virions contain normal quantities of each viral protein, including the REN-P fusion protein (Fig. 3B). To determine whether the REN-P protein is enzymatically active, we lysed purified virions in the presence of *Renilla* luciferase substrate. We detected luminescence that increased in proportion to the quantity of virus particles over a 500-fold range (Fig. 3C). Thus, the REN-P fusion protein is a functional luciferase enzyme that allows direct quantification of virus particle number.

ε-COP depletion reduces the efficiency of VSV attachment. We adapted the method of particle quantification to create an enzymatic assay for viral attachment. Cells were exposed to VSV REN-P for 1 h at 4°C, and unbound virus was removed by washing. The virus-cell complexes were lysed in the presence of substrate, and luminescence was quantified. We found that 0.5 to 5% of input virions bound to cells at 4°C, and the quantity of attached virions increased proportionally with the amount of input virus (Fig. 3D). Such low-level, nonsaturable binding is in good agree-

TABLE 1 Effects of individual siRNAs on cell viability and VSV infection

Targeted gene and siRNA	% Total cells (mean ± SD)[a]	% Infected cells (mean ± SD)[a]	Dharmacon catalog no.
Beta-COP			
siRNA 1	112 ± 29	78 ± 39	D-017940-01
siRNA 2[b]	115 ± 4	55 ± 5	D-017940-02
siRNA 3	90 ± 9	79 ± 9	D-017940-03
siRNA 4	110 ± 4	90 ± 9	D-017940-04
Delta-COP			
siRNA 1	99 ± 8	64 ± 9	D-013063-01
siRNA 2[b]	84 ± 4	33 ± 5	D-013063-02
siRNA 3[b]	76 ± 21	48 ± 11	D-013063-03
siRNA 4[b]	76 ± 16	34 ± 17	D-013063-04
Gamma1-COP			
siRNA 1	72 ± 11	102 ± 1	D-019138-01
siRNA 2	54 ± 2	78 ± 4	D-019138-02
siRNA 3[b]	95 ± 6	55 ± 5	D-019138-03
siRNA 4	66 ± 28	80 ± 4	D-019138-04
Zeta1-COP			
siRNA 1	57 ± 24	95 ± 2	D-020293-01
siRNA 2	61 ± 14	32 ± 8	D-020293-02
siRNA 3	59 ± 26	63 ± 14	D-020293-03
siRNA 4[b]	94 ± 20	41 ± 11	D-020293-04
Zeta2-COP			
siRNA 1	92 ± 8	109 ± 4	D-021116-01
siRNA 2	122 ± 9	82 ± 3	D-021116-02
siRNA 3	83 ± 4	103 ± 4	D-021116-03
siRNA 4[b]	96 ± 3	31 ± 9	D-021116-04

[a] Values are expressed as percentages of the total or infected cells in untreated (buffer control) samples infected with VSV-eGFP.
[b] siRNA that significantly reduced VSV infection without reducing cell viability.

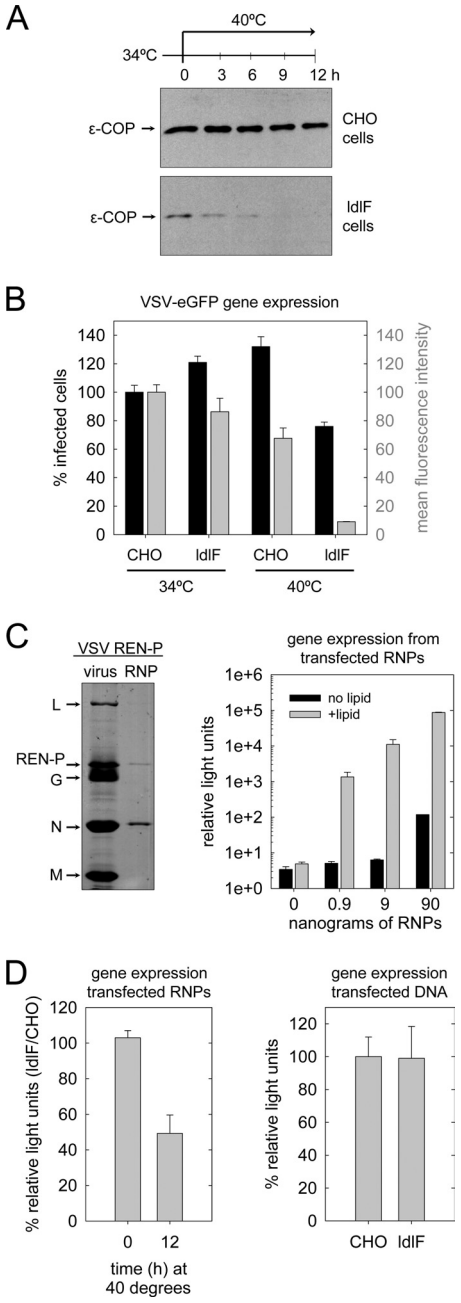

FIG 2 ε-COP depletion inhibits the early stages of VSV replication. (A) Western blot analysis of ε-COP levels in wt and ldlF cells. ε-COP was detected using polyclonal antisera following SDS-PAGE of 10 μg of a total cell lysate prepared from wt or ldlF cells after shifting the cells to 40°C for the indicated time interval. (B) Effect of ε-COP depletion on VSV-eGFP entry and gene expression. CHO and ldlF cells were incubated for 12 h at 34°C or 40°C and inoculated with VSV-eGFP (MOI, 1). After 7 h at the indicated temperature, the percentage of eGFP-positive cells (black) and the mean eGFP fluorescence intensity (gray) in each cell population was quantified by flow cytometry. Data are expressed relative to those obtained in CHO cells at 34°C (set to 100%). Values are the means ± SDs from triplicate samples in a single experiment. (C) Assay for gene expression from transfected RNPs. Left, Coomassie blue-stained SDS-polyacrylamide gel of RNPs isolated from VSV REN-P virions. Right, gene expression from transfected RNPs. The indicated quantity of RNPs was complexed with Lipofectamine 2000 (+lipid) or left untreated (no lipid). CHO cells were inoculated with the RNP solutions, and the cells were maintained at 37°C. At 5 h posttransfection, luminescence was quantified as described in Materials and Methods. Values are the means ± SDs for duplicate samples in a single representative experiment. (D) Effect of ε-COP depletion on gene expression from transfected RNPs. CHO and ldlF cells were incubated at 40°C for 0 h (34°C) or 12 h and transfected with 9 ng of VSV REN-P RNPs (left panel) or 40 ng of plasmid DNA encoding *Renilla* luciferase (right panel). At 5 h posttransfection, cells were lysed in the presence of *Renilla* luciferase substrate, and luminescence was quantified immediately after lysis. Values are the means ± SDs from a single representative experiment (RNPs) or from duplicate experiments (DNA). The raw values obtained for RNP-transfected cells were similar to those shown in panel C for cells transfected with 9 ng of RNPs.

ment with measurements obtained using radiolabeled virus (data not shown) (41, 42). Virus attachment was G protein dependent, as pretreatment of virus with a neutralizing monoclonal antibody (IE2) directed against VSV G (62) or proteolytic removal of G protein from particles reduced the cell-associated enzyme activity by >80% (Fig. 3E). Following ε-COP depletion, virus binding to ldlF cells was diminished by 40% (Fig. 3F). In contrast, similar numbers of VSV REN-P particles bound to wt and ldlF cells maintained at 34°C. Thus, ε-COP depletion reduces the efficiency of VSV attachment.

Depletion of ε-COP inhibits a postattachment step of VSV entry. The moderate defect in VSV attachment suggested that a downstream step of entry may also be compromised by coatomer inactivation. Thus, we used VSV REN-P to develop a real-time assay that detects the final step of virus entry, cytosolic RNP release. We treated CHO cells with puromycin to prevent translation of newly transcribed REN-P mRNAs and loaded the cells with a membrane-permeable substrate for *Renilla* luciferase (EnduRen). Inoculation of cells with VSV REN-P (MOI, 25) led to an 8- to 10-fold increase in the cell-associated luminescence by 120 min p.i. (Fig. 4A and B). This increase in luminescence depended on viral membrane fusion and access of RNPs to EnduRen in the cell cytosol, since preventing endosome acidification with NH_4Cl or bafilomycin A1, or preincubation of virions with a neutralizing antibody, resulted in background levels of luminescence (Fig. 4A and B). To confirm that the enzyme activity was not simply a result of new viral protein synthesis, we irradiated purified VSV REN-P with UV light to block transcription of the viral genome. A dose of 820 ergs mm^{-2}, which inhibits synthesis of all viral mRNAs (5, 66), did not reduce the luciferase activity of the REN-P protein or the luminescence increase observed in puromycin-treated cells. However, under conditions permissive for viral gene expression (i.e., in the absence of puromycin), this dose of irradiation decreased luminescence by >95% compared to that of samples infected with nonirradiated virions (Fig. 4C). These data confirm that the measured luminescence in puromycin-treated cells does not depend upon new viral gene expression. Thus, VSV REN-P permits a quantitative, kinetic analysis of RNP release that is not influenced by the significantly downstream steps of viral gene expression.

Next, we used the enzymatic RNP release assay to quantify the effect of coatomer inactivation on the overall efficiency of VSV entry. We found that ε-COP depletion in ldlF cells reduced VSV REN-P entry to the limit of detection (Fig. 4D and E). Importantly, the low signal detected in the ldlF cells was not due to a decreased capacity of the cells to convert EnduRen into an active substrate for the REN-P enzyme (Fig. 4F). Thus, these observations show that ε-COP depletion dramatically inhibits VSV entry during or before the step of RNP release from endosomal compartments.

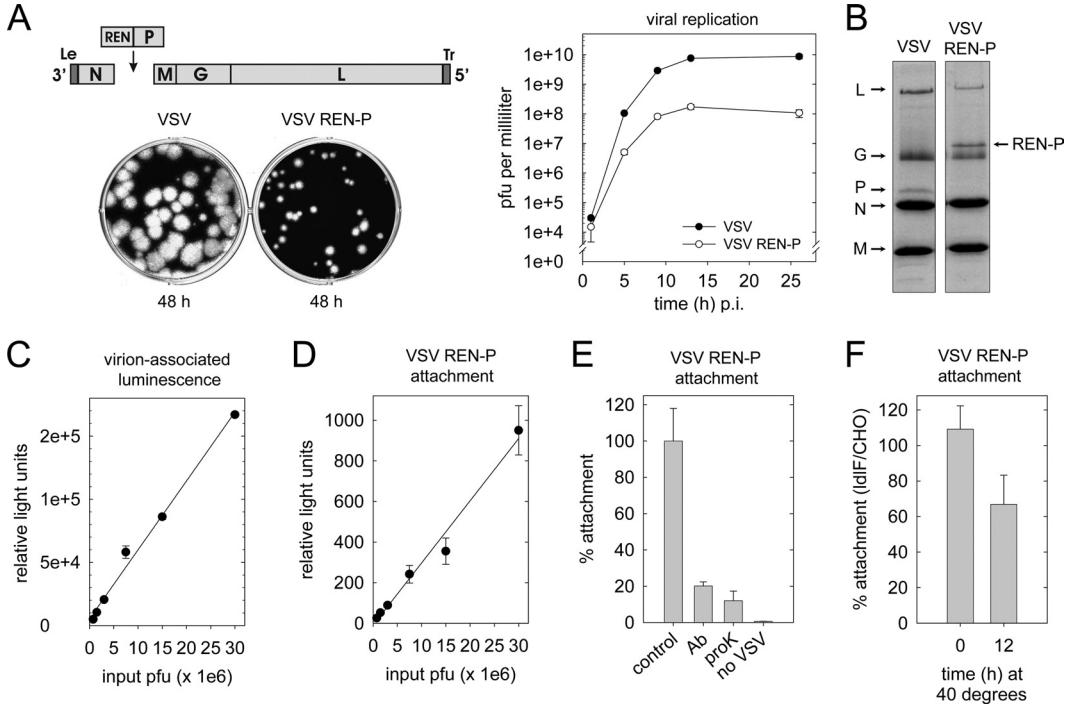

FIG 3 VSV REN-P: an enzymatic reporter of virus particle number. (A) Biological properties of VSV REN-P. Top left, schematic of the VSV REN-P genome. The 5 major open reading frames are delimited by vertical lines and labeled with capital letters that correspond to the gene product. The noncoding leader (Le) and trailer (Tr) regions flank the coding portions of the genome. Lower left, plaque morphologies of VSV and VSV REN-P at 48 h p.i. of Vero cells. Right, single-step growth kinetics of VSV and VSV REN-P. BHK-21 cells were infected at an MOI of 3, and the titer of virus released from the cells at each time point was measured by plaque assay on Vero cells. Data points are the averages ± SDs for duplicate samples from a single representative experiment. (B) Coomassie blue-stained SDS-polyacrylamide gel of purified VSV and VSV REN-P particles. (C) Luciferase activity associated with purified VSV REN-P particles. The indicated quantity of virus was lysed in the presence of *Renilla* luciferase substrate, and luminescence was measured immediately. Data points are the means ± SDs from 2 independent experiments. (D) Virus attachment. CHO cells were exposed to the indicated quantity of VSV REN-P at 4°C for 1 h, and unbound virus was removed by washing. Attached virions were lysed in the presence of substrate, and luminescence was quantified immediately. Data points are the means ± SDs from 2 experiments. (E) Effect of virus neutralization and G protein cleavage on VSV REN-P attachment. Virions were treated with a neutralizing antibody (IE-2) directed against G protein or proteinase K (proK) prior to incubation with cells as for panel D. The means ± SDs for triplicate samples in a single representative experiment are shown. (F) Effect of ε-COP depletion on VSV attachment. CHO and ldlF cells were incubated for 0 or 12 h at 40°C, and cells were rapidly shifted to 4°C and inoculated with VSV REN-P (MOI, 250). Following a 1-h adsorption at 4°C, unbound virus was removed by washing, and the amount of bound virus was measured as for panel D. The means ± SDs from 4 independent experiments are plotted as the percentage of relative light units observed in ldlF cells divided by that observed in wt CHO cells under the same conditions.

Coatomer inactivation inhibits VSV internalization. To directly measure the effect of coatomer inactivation on viral endocytosis, we quantified the rate of VSV internalization at the levels of single cells and individual virus particles. We exposed cells to Alexa 647-labeled VSV particles, and following cell fixation, we immunostained the surface-bound particles using a spectrally separable fluorophore. We then acquired images that spanned the volume of individual cells (Fig. 5A) and counted the number of internal particles in each cell (Fig. 5B). Depletion of ε-COP levels in ldlF cells decreased the rate and overall efficiency of virus internalization (Fig. 5A and B). Moreover, ldlF cells consistently contained fewer attached particles at early times and a higher ratio of external to internal particles than wt cells at all time points (Fig. 5A). These data confirm that ε-COP depletion in ldlF cells reduces the efficiency of VSV attachment and reveal a separate defect in virus internalization.

To determine if inhibition of coatomer function decreases the uptake of clathrin-dependent cargos other than VSV, we incubated wt and ldlF cells for 12 h at 40°C and assessed the capacity of the cells to take up fluorescent transferrin (Tf). Indeed, Tf uptake was severely compromised in ldlF cells, while the wt cells efficiently internalized ligand (Fig. 5C). These observations show that coatomer inactivation in ldlF cells decreases the uptake efficiencies of two different clathrin-dependent cargos.

VSV RNP release does not require COPI function. To determine whether the few virus particles endocytosed by ldlF cells could release their RNPs from endosomes, we developed a visual assay using VSV particles in which the RNP core was tagged with eGFP (VSV-eGFP-P) (55) and the G proteins were labeled with Alexa Fluor 647 (A647-G). Images of the dually labeled particles on glass showed that approximately 90% of the particles contained both fluorophores (Fig. 6A and G).

To assay for RNP release from the dually labeled particles, we induced the synchronous uptake of virus prebound at 4°C and measured the fraction of particles that had undergone RNP release (as evident by the separation of the G-associated AF647 and RNP-core associated eGFP fluorescence) with respect to time. We found that RNP translocation was rapid and efficient in wt CHO cells and ldlF cells depleted of ε-COP, as the number of intracellular A647-G spots that were eGFP positive rapidly decreased from >90% at the time of temperature shift to <20% by 30 min in both cellular contexts (Fig. 6B, C, F, and G). As expected, separa-

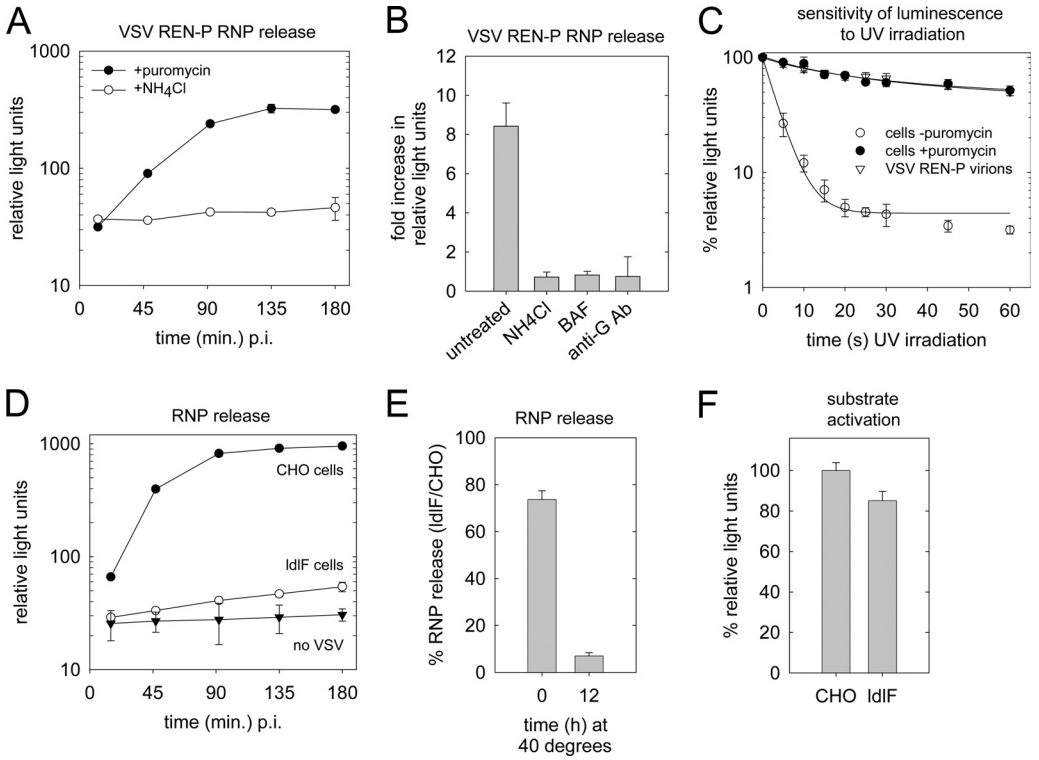

FIG 4 Enzymatic detection of release of the RNP core. (A) Enzymatic detection of VSV RNP release. CHO cells were preloaded with EnduRen for 1.5 h at 37°C and treated with 50 μg/ml puromycin (●) or 20 mM NH_4Cl (○) for the final hour of substrate loading. Cells were inoculated with VSV REN-P (MOI, 25), and the luminescence emitted from live cells was measured at the indicated intervals. Values are the averages ± SDs for triplicate samples in a single experiment. (B) Effect of virus neutralization or endosome acidification on VSV REN-P RNP release. CHO cells were loaded with EnduRen for 1.5 h at 37°C and treated with 50 μg/ml puromycin for the final hour of substrate loading. Thirty minutes prior to virus addition, cells were exposed to 20 mM NH_4Cl or 100 nM BAF or left untreated. Cells were inoculated with VSV REN-P (MOI, 25) or virus that had been preincubated with a neutralizing antibody against VSV G for 1 h at 37°C (anti-G Ab). The luminescence emitted from live cells in duplicate samples was quantified at 5 min and 120 min after virus addition in each experiment. The fold increase in relative light units from 5 min to 120 min was calculated and expressed as mean ± SD from samples in six experiments (untreated), five experiments (NH_4Cl), or single experiments (BAF and anti-G Ab). (C) Effect of UV irradiation on viral gene expression and RNP release. Purified VSV REN-P particles were exposed to UV light at 41 ergs mm^{-2} s^{-1} for the indicated time intervals. CHO cells were loaded with EnduRen and inoculated with virus at a preirradiation MOI of 25. Luminescence was measured following 3 h at 37°C in the presence (●) or absence (○) of 50 μg/ml puromycin. As a control for UV-mediated damage of the REN-P enzyme, the enzyme activity of particles irradiated for the same time intervals was measured directly following lysis and exposure of the particles to substrate (▽). Results for irradiated samples are expressed as a percentage of that for unirradiated samples tested under the same conditions. Plotted values are the averages ± SDs from 2 experiments. (D) Effect of ε-COP depletion on VSV RNP release. CHO (●) and ldlF (○) cells were incubated at 40°C for 10.5 h and loaded with EnduRen and 50 μg/ml puromycin for 1.5 h and 1 h, respectively. Cells were inoculated with VSV REN-P (MOI, 25), and luminescence was measured at the indicated times p.i. The means ± SDs for triplicate samples in a single experiment are shown. (▼), luminescence of cells alone loaded with substrate. (E) Quantitation of RNP complex release. Triplicate samples of CHO and ldlF cells were incubated for 0 or 10.5 h at 40°C and treated as for panel D. The mean luminescence in ldlF cells at 90 min p.i. was expressed as a percentage of that observed in CHO cells under similar conditions, and the plot shows the average percentage ± SD from 3 independent experiments. (F) EnduRen activation efficiency. CHO and ldlF cells were incubated for 10.5 h at 40°C and loaded with EnduRen for 1.5 h. The capacity of cells to convert EnduRen to a substrate for the REN-P enzyme was evaluated by lysing the loaded cells in the presence of 1×10^8 PFU of VSV REN-P. Luminescence was plotted as the mean ± SD from 2 experiments.

tion of the eGFP signal did not occur in cells pretreated with NH_4Cl (Fig. 6E and G). Detection of the viral nucleocapsid protein by immunofluorescence (IF) microscopy also revealed a loss of P that occurred during RNP release, as most cytosolic RNPs lacked detectable eGFP signal (Fig. 6D). Thus, our combined results demonstrate that ε-COP depletion in ldlF cells primarily inhibits the attachment and internalization steps of VSV entry and not viral membrane fusion or RNP release.

We reasoned that the location of the A647-G spots might correspond to the endosomal location of RNP release. Therefore, we costained ldlF cells with an antibody against a marker of early endosomes, early endosomal antigen 1 (EEA1). As early as 10 min after the temperature shift, we observed the colocalization of A647-G spots lacking eGFP-P with EEA1 (Fig. 6H), demonstrating that viral fusion and RNP release can occur from an early endosome.

Prolonged chemical inhibition of coatomer function impairs VSV entry. Given the effect of ε-COP depletion on cellular endocytosis, we sought to test whether a short-term chemical inhibition of COPI function results in a similar phenotype. Brefeldin A (BFA), a small-molecule inhibitor of COPI-dependent membrane transport, prevents the Arf1-dependent recruitment of coatomer to cellular membranes (54) and rapidly induces fragmentation of the Golgi apparatus. BFA is known to inhibit VSV RNA synthesis (28), but the effect of BFA on VSV entry was unknown. Consistent with previous results, we found that BFA treatment of CHO cells for 1 h or 12 h reduced gene expression from transfected VSV REN-P RNPs by 70% or 95%, respectively (Fig. 7A). Treatment of

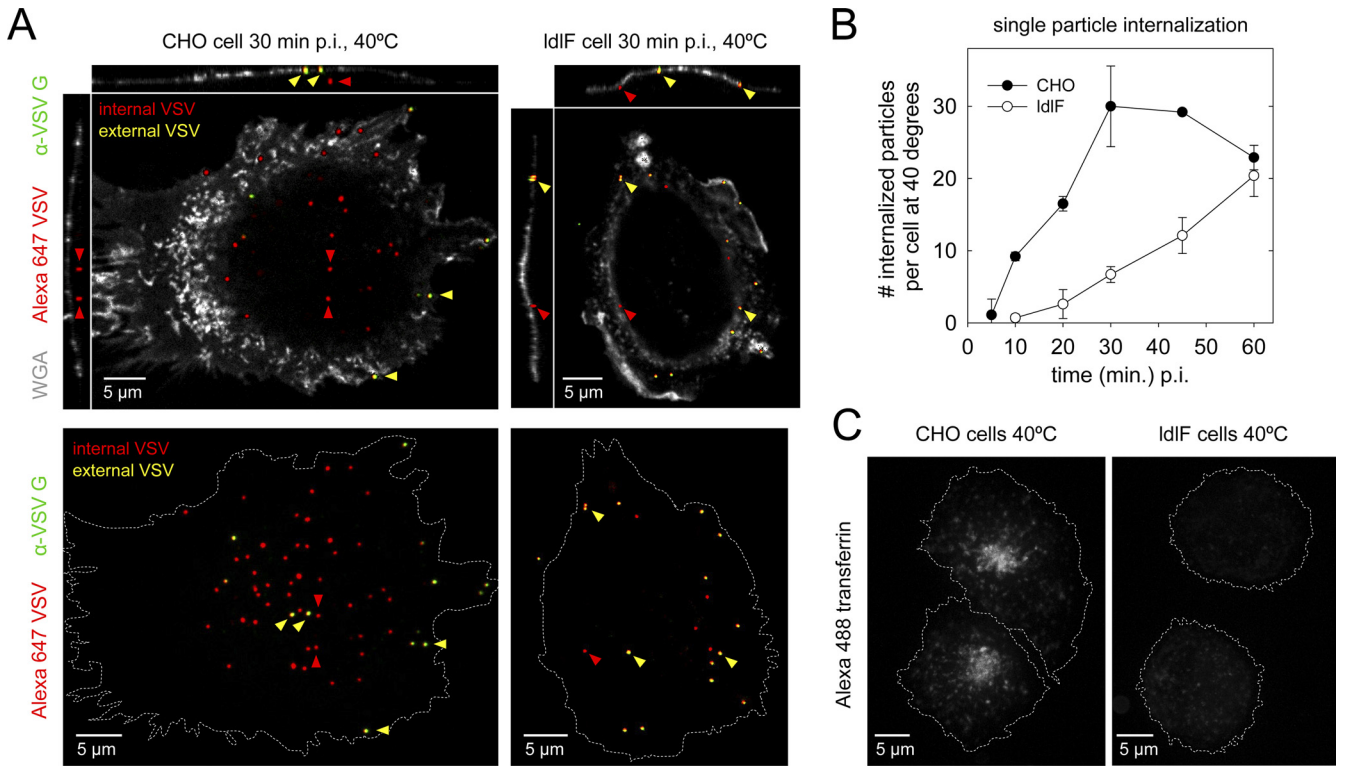

FIG 5 ε-COP depletion inhibits VSV internalization. (A) Antibody accessibility assay for quantifying internalized VSV particles. CHO (left) and ldlF (right) cells were incubated for 12 h at 40°C prior to inoculation with Alexa 647 VSV particles (red; MOI, 500). Cells were fixed at 30 min p.i., and the glycans on the cell surface were labeled with wheat germ agglutinin (WGA) (gray). Surface-bound virions (yellow) were detected with an antibody specific for VSV G and an Alexa Fluor 488-labeled secondary antibody. Image sections encompassing the entire cell volume were acquired every 0.5 μm by confocal microscopy. Top panels, single planes acquired from the midplanes of individual CHO and ldlF cells. Panels to the left and above each primary image show a 3× interpolation of the cell volume in the *x* or *y* dimension, respectively. Lower panels, projected image of all focal planes from the cells shown above. Yellow or red arrowheads indicate external or internal particles. The same particles are highlighted in the upper and lower panels. The dashed white line indicates the outermost cell boundary. (B) Kinetics of VSV internalization in CHO and ldlF cells. Cells were treated as for panel A and fixed at the indicated time points. The number of internalized particles per cell was measured for 20 cells per time point and averaged. The data points are means of the average counts ± SDs from 2 experiments. (C) Effect of ε-COP depletion on transferrin uptake. CHO and ldlF cells were incubated for 12 h at 40°C and pulsed with Alexa 488 transferrin for 5 min. Surface-bound transferrin was removed by a brief acid wash, and the cell surface was stained with WGA prior to image acquisition. Images were acquired as for panel A, and a projected image of all the planes is shown for the transferrin signal alone. The dashed white line indicates the outer cell boundary.

CHO cells for 1 h with BFA did not impair VSV adsorption (data not shown) or RNP release (Fig. 7B). However, incubation of cells with BFA for 12 h inhibited VSV entry and RNP release by 80% (Fig. 7B). Prolonged treatment of cells with BFA also blocked Tf internalization, while shorter durations of drug treatment decreased Tf uptake to a lesser extent (Fig. 7C). As expected, this short-term BFA treatment caused Golgi fragmentation (Fig. 7C). Together, our data show that prolonged chemical and genetic inhibition of coatomer function prevents efficient VSV entry and Tf uptake. However, short-term disruption of COPI-dependent membrane transport has little to no effect on the endocytic transport of these cargos, indicating that the long-term effects of coatomer inactivation are likely indirect.

DISCUSSION

In the present study, we examined how inhibition of COPI-dependent membrane transport impairs the early stages of VSV infection. We show that genetic depletion of ε-COP separately impaired virus endocytosis and gene expression without inhibiting RNP release by internalized particles. However, chemical inactivation of coatomer function showed that VSV entry was affected only by long-term treatment of cells with BFA. Thus, our observations support the following conclusions: (i) COPI function is critical for efficient VSV internalization and gene expression, (ii) COPI activity is not required for VSV membrane fusion or RNP release, and (iii) long-term COPI inactivation perturbs cellular membrane traffic and thereby indirectly reduces the efficiency of VSV attachment and endocytosis.

Genetic depletion of ε-COP in ldlF cells primarily inhibited VSV endocytosis. Given that the downstream steps of viral membrane fusion and RNP release were not impaired in ldlF cells, we conclude that the magnitude of this endocytic defect is sufficient to account for the overall reduction in virus entry that we observed using the enzymatic assay for RNP release. We further show that this endocytic defect was not unique to VSV, as Tf uptake was also reduced by ε-COP depletion in ldlF cells. This observation agrees with data from earlier studies that reported a partial defect in Tf uptake in human cells treated with siRNAs against β-COP for 48 h (52) and in ldlF cells preincubated at 40°C for 8 h (16). The latter study also demonstrated that ε-COP depletion prevents the delivery of another clathrin-dependent cargo, Semliki Forest virus (SFV), to acidified endosomes (16). This SFV entry block was

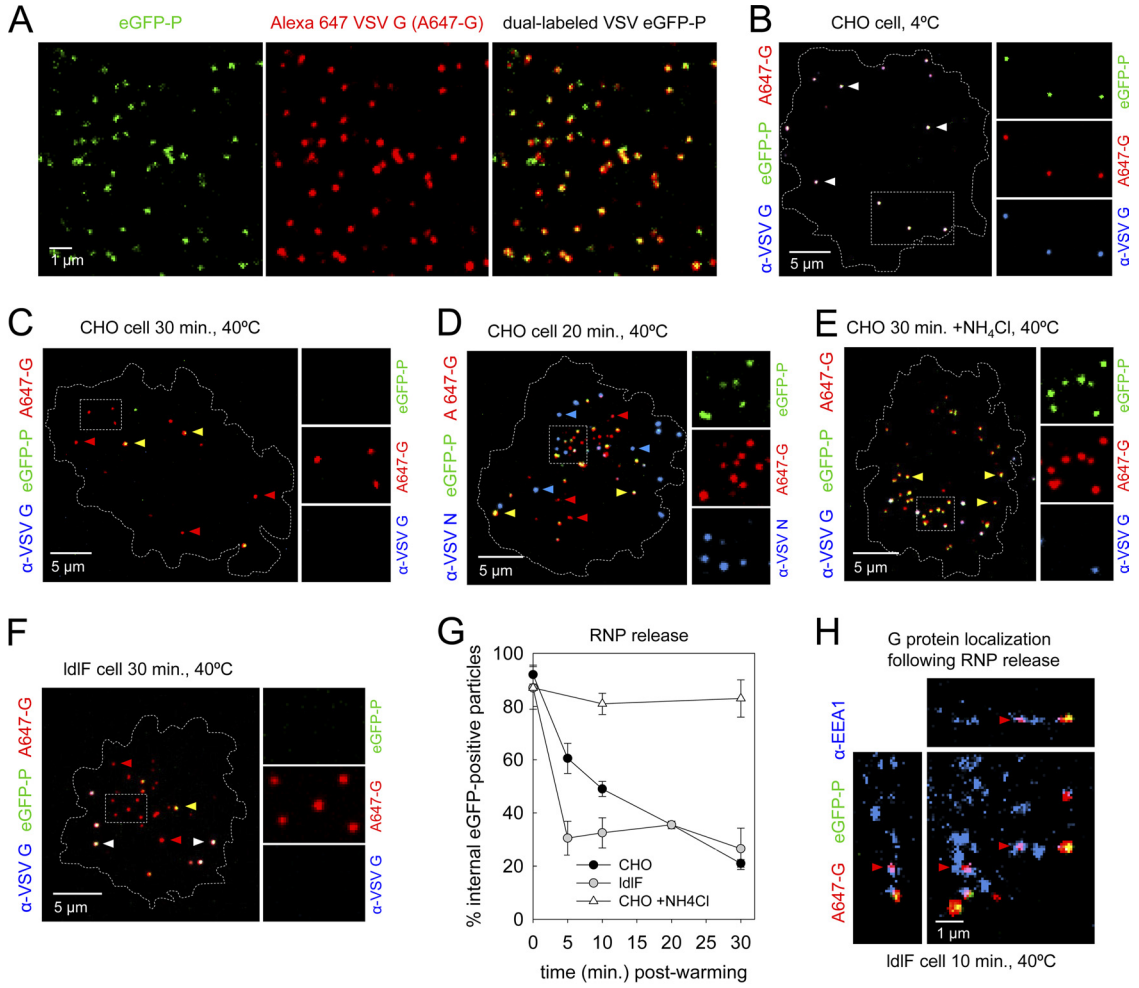

FIG 6 VSV RNP release does not require COPI function. (A) Images of VSV-eGFP-P virions labeled with Alexa Fluor 647 (A647-G). Particles were nonspecifically adsorbed to a glass coverslip, and images were acquired using a spinning-disk confocal microscope. Images of the eGFP-P (left) and Alexa dye (middle) channels are shown next to a channel overlay (right). (B) Visualization of attached VSV eGFP-P particles. CHO cells were incubated with dually labeled particles (MOI, 500) for 1 h at 4°C. Unbound virions were removed by washing, and following fixation, the extracellular particles were visualized by IF detection of anti-VSV G primary antibodies with an Alexa 594-labeled secondary antibody (blue). Optical sections of cells were acquired by confocal microscopy as for Fig. 5A, and a projected image of planes encompassing a single cell is shown on the left. The white dashed line delimits the outer cell boundary. White arrowheads highlight external, triple-colored virus particles. Right panels, expanded single-channel views of the boxed region at left. (C) Visual detection of VSV-eGFP-P uncoating. CHO cells were incubated at 40°C for 12 h, and virus entry was synchronized by first binding dually labeled particles to cells at 4°C (see panel B). Virion uptake was activated by rapidly shifting the virus-cell complexes to 40°C, and samples were fixed after 30 min. Surface-bound virions were detected by IF, and images were acquired and presented as for panel B. Red arrowheads, internalized particles that have released their RNPs. Yellow arrowheads, internalized virions that contain RNPs. (D) Location of VSV RNPs after particle entry. Dual-colored particles were incubated with cells for 20 min as described for panel C. N protein was detected by IF, and images were acquired and displayed as for panel B. Arrowheads indicate spots of Alexa 647 G that do not contain N protein (red), spots of N protein that lack G (blue), and internal particles that still contain an RNP (yellow). (E) Effect of NH_4Cl on particle uncoating. CHO cells were incubated for 12 h at 40°C, and NH_4Cl was added to 20 mM at 11.5 h. Dual-colored particles were allowed to synchronously enter cells for 30 min (see panel C) in the presence of NH_4Cl. Surface-bound virions were detected by IF, and three-dimensional (3D) images were acquired as for panel B. Yellow arrowheads, internal particles containing an RNP. (F) VSV RNP release in ldlF cells. Cells were incubated at 40°C for 12 h and allowed to synchronously take up dual-colored particles for 30 min (see panel C). Cells were inoculated with 4-fold more virus than the cells in panel B to ensure that a similar number of particles were taken into both cell types. Extracellular particles were detected by IF, and images were acquired as for panel B. Arrowheads highlight uncoated (red), intact (yellow), and extracellular (white) particles. (G) Kinetics of VSV RNP release. CHO and ldlF cells were incubated at 40°C for 12 h. Dual-colored particles were allowed to synchronously enter cells for the indicated times in the presence (see panel E) or absence of NH_4Cl. ldlF cells were inoculated with 4-fold more virus than CHO cells to ensure similar numbers of internalized particles per cell in both cell types. Extracellular virions were detected by IF, and images were acquired as described for panel B. The percentage of intracellular particles containing eGFP-P was measured for at least 12 individual cells per time point, and the percentages at each time point were averaged. Data points are the means ± SDs of the average percentages from 2 experiments. (H) Evidence for RNP release from early endosomes. Dual-colored particles were allowed to synchronously enter ldlF cells for 10 min at 40°C. Early endosomes were detected by IF using antibodies against EEA1 (blue). 3D image sets were acquired as for panel B, and a single focal plane from an individual cell is shown. Red arrowheads indicate the positions of Alexa 647 spots that colocalize with EEA1 and do not contain detectable eGFP-P. Images to the left and top of the main panel show 3× interpolated images of the cell volume in the *x* and *y* dimensions, respectively.

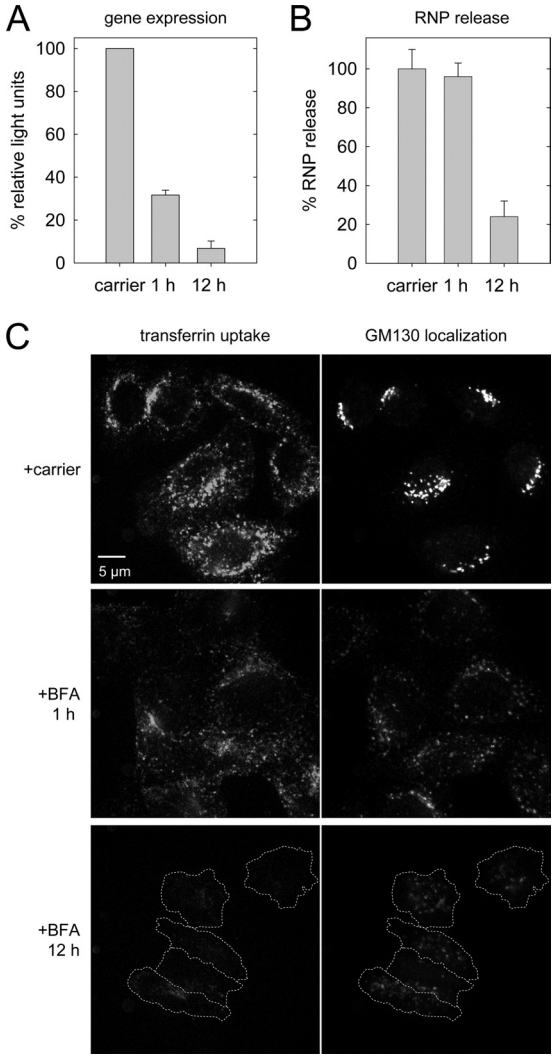

FIG 7 Prolonged treatment of cells with brefeldin A inhibits VSV entry. (A) Effect of BFA treatment on VSV gene expression. CHO cells were treated with ethanol carrier or 5 μg/ml BFA for 1 h or 12 h. Cells were transfected with VSV REN-P RNPs in the presence of compound, and luminescence was quantified after incubation of the samples at 37°C for 5 h. Values are the means ± SDs from two independent experiments and are expressed as a percentage of the value for the carrier control samples. (B) Effect of BFA treatment on VSV RNP release. Left, CHO cells were treated with ethanol carrier or 5 μg/ml BFA for 1 h or 12 h at 37°C. Treated cells were incubated with EnduRen for 1.5 h and puromycin for 1 h prior to addition of virus. Cells were inoculated with VSV REN-P (MOI, 25) in the presence of compound, and luminescence was quantified at 90 min. p.i. Data points are the means ± SDs from two independent experiments and are expressed as a percentage of the value for the carrier control samples. (C) Effect of BFA on Tf uptake. CHO cells were treated with ethanol carrier or 5 μg/ml BFA for 1 h or 12 h at 37°C. Treated cells were incubated with 40 μg/ml Alexa 488 human Tf (green) in the presence of compound for 5 min at 37°C. Extracellular Tf was removed by acid wash, and cells were fixed and stained for GM130. Dotted lines in the lower panels indicate the cell periphery.

attributed to a defect in endosomal sorting of the virus particles. However, it is plausible that SFV particles could not be detected in acidified endosomes because they were inefficiently internalized from the cell surface.

Since the COPI machinery does not directly participate in the clathrin-dependent uptake of VSV or Tf, our findings suggest that coatomer inactivation indirectly perturbs clathrin-dependent endocytosis or ligand binding to the cell surface. To our knowledge, coatomer depletion has not been shown to directly affect the clathrin endocytic process. However, low-density lipoprotein receptors (LDLR) are rapidly depleted from the surface of ldlF cells upon ε-COP depletion (27), which implies that the surface levels of other receptor proteins may also change in ldlF cells. In the case of transferrin receptors (TfR), ε-COP depletion for 8 h did not induce TfR degradation or alter the steady-state ratio of surface to internal receptor (16). However, we cannot exclude the possibility that fewer TfRs remained on the surface of ldlF cells after the longer duration of ε-COP depletion used here.

In the case of VSV, we found that inhibiting COPI function reduced particle attachment to cells by ~30%. The magnitude of this defect was not sufficient to account for the overall reduction in virus internalization, indicating that ε-COP depletion reduces both virus attachment and internalization. The effect of coatomer inactivation on VSV adsorption likely reflects changes in the abundance of proteins or lipids or their modification status at the plasma membrane of ldlF cells. Considering that electrostatic interactions are thought to be sufficient for VSV attachment (4, 10), it is difficult to pinpoint which alterations in cell surface composition might impair virus binding. A recent study demonstrated that RNAi-mediated depletion of γ-COP in HeLa cells partially redistributed cholesterol and GM1 sphingolipids from the plasma membrane to an intracellular compartment (45). Addition of cholesterol and GM1 to the coatomer-depleted cells in *trans* modestly increased plasma membrane ruffling induced by *Salmonella* bacteria and the susceptibility of the cells to VSV infection (45), indicating that alterations to lipid localization directly or indirectly contribute to the decreased efficiency of VSV infection in cells with reduced coatomer levels.

The effects we observed on VSV attachment and endocytosis resulted from prolonged inhibition of coatomer function. We base this conclusion on the observations that pretreatment of cells with BFA for 1 h did not inhibit VSV attachment or entry and likewise had little effect on Tf uptake, while BFA treatment for 12 h reduced the efficiency of VSV entry by 80% and dramatically inhibited Tf endocytosis. Since BFA induces Golgi fragmentation within minutes and clearly caused the redistribution of GM130 by 1 h in CHO cells, our data indicate that VSV entry does not require COPI function directly.

There are 2 models of VSV membrane fusion and RNP release. In one model, VSV virions fuse with the limiting membrane of an EE, which directly releases the RNP into the cell cytosol. According to the second model, VSV particles fuse with vesicles inside multivesicular bodies (MVBs), an endosomal intermediate between EEs and LEs (32). Release of the entrapped RNPs then requires delivery of the internal vesicles into a LE and vesicle back fusion with the LE limiting membrane (32). Because coatomer inactivation in ldlF cells inhibits formation of intraluminal vesicles (21) and the efficiency of endocytic cargo accumulation in LEs and lysosomes (16, 21), there should be a specific defect in VSV RNP release. Our data are not consistent with this second route of entry, since most VSV particles prebound to wt or ldlF cells completed RNP release 10 min after warming of the virus-cell complexes. Rather, the rapid kinetics of RNP release that we observed agrees with previous reports showing that VSV particles reach and penetrate acidic endosomal compartments within 5 min of uptake (29, 43, 44). The kinetics of this process is also consistent with

release of RNPs from EEs, as is the detection of G protein in EEs of ldlF cells that lacked detectable RNP signal. Thus, our data provide further support for the conventional model of VSV entry from EEs.

Genetic and chemical inactivation of coatomer function decreased viral gene expression. Given that ε-COP depletion in ldlF cells does not inhibit protein translation (27) and BFA treatment does not significantly affect VSV protein synthesis (28), the block to viral gene expression likely occurs at the level of viral RNA synthesis. Our results agree with the prior finding that BFA inhibited VSV RNA synthesis when cells were treated with the compound at 2 or 4 h after exposure of cells to virus (28). Under these conditions, BFA decreased the abundance of viral transcripts and genomic replication products, so it is unclear whether BFA treatment specifically impaired one or both of these RNA synthetic processes. Although we cannot exclude the possibility that BFA may directly inhibit RNA synthesis by the viral RdRp, the similar effects of BFA treatment and ε-COP depletion on VSV gene expression suggest that their inhibitory effect results from changes to cellular factors that modulate viral RNA synthesis.

Positive-strand RNA viruses are well known to replicate on intracellular membrane-bound organelles, including vesicles generated by the COPI system (13, 19). In contrast, the replication machinery of VSV does not appear to localize to a membranous compartment. Rather, the input RNP cores can synthesize RNA throughout the cytoplasm, and following protein synthesis, the RNA synthetic machinery localizes to cytosolic inclusions that are the sites of viral transcription (25). Although the inclusions can become loosely surrounded by membrane bilayers, this association is not required for viral RNA synthesis, as it occurs late in the infection cycle (>8 h p.i.) (25). This apparent membrane wrapping of VSV inclusions could result from displacement of existing cellular membranes (e.g., ER membranes) as the inclusions expand or from an active cellular process triggered by the virus (e.g., autophagy). Indeed, VSV infection can induce autophagy in mammalian and *Drosophila melanogaster* cells (33, 56), and coatomer activity was recently shown to be important for autophagosome maturation in mammalian cells (52). However, the autophagic response induced by VSV apparently modulates viral replication differently in the two systems (30, 56). Thus, it remains uncertain how coatomer inactivation perturbs VSV gene expression and whether alterations to cellular autophagy contribute to the inhibitory phenotype.

At the outset of our study, COPI coatomer was known to play a critical role in biosynthetic membrane transport and was implicated in endocytic transport. With such central roles for COPI in directing membrane traffic, it is perhaps unsurprising that many RNAi-based screens designed to identify host susceptibility factors for pathogenic microbes have included the coatomer complex as a hit. Here we demonstrate that COPI inactivation reduces viral attachment and internalization as a secondary consequence of changes to the plasma membrane. The fact that release of the viral RNP core into cells is unaffected by coatomer depletion shows that COPI-dependent endocytic transport is not required for VSV infection. Resolving the potential effects of coatomer inactivation on VSV endocytosis and RNP release required the development of quantitative assays that directly visualize the progression of individual virions through the endocytic pathway. These assays will facilitate further analysis of VSV entry and, importantly, the entry of VSV particles pseudotyped with other viral envelope proteins. Due to the complex phenotypes caused by depletion of cellular membrane transport factors, we anticipate that similar analyses will be critical for discerning how pathogens exploit coatomer and other such factors to invade target cells.

ACKNOWLEDGMENT

This work was supported by NIH grant AI081842 to Sean P. J. Whelan.

REFERENCES

1. **Agaisse H, et al.** 2005. Genome-wide RNAi screen for host factors required for intracellular bacterial infection. Science **309**:1248–1251.
2. **Akimana C, Al-Khodor S, Abu Kwaik Y.** 2010. Host factors required for modulation of phagosome biogenesis and proliferation of Francisella tularensis within the cytosol. PLoS One **5**:e11025.
3. **Aniento F, Gu F, Parton RG, Gruenberg J.** 1996. An endosomal beta COP is involved in the pH-dependent formation of transport vesicles destined for late endosomes. J. Cell Biol. **133**:29–41.
4. **Bailey CA, Miller DK, Lenard J.** 1984. Effects of DEAE-dextran on infection and hemolysis by VSV. Evidence that nonspecific electrostatic interactions mediate effective binding of VSV to cells. Virology **133**: 111–118.
5. **Ball LA, White CN.** 1976. Order of transcription of genes of vesicular stomatitis virus. Proc. Natl. Acad. Sci. U. S. A. **73**:442–446.
6. **Beck R, Rawet M, Wieland FT, Cassel D.** 2009. The COPI system: molecular mechanisms and function. FEBS Lett. **583**:2701–2709.
7. **Bethune J, Wieland F, Moelleken J.** 2006. COPI-mediated transport. J. Membr. Biol. **211**:65–79.
8. **Brass AL, et al.** 2009. The IFITM proteins mediate cellular resistance to influenza A H1N1 virus, West Nile virus, and dengue virus. Cell **139**: 1243–1254.
9. **Buchholz UJ, Finke S, Conzelmann KK.** 1999. Generation of bovine respiratory syncytial virus (BRSV) from cDNA: BRSV NS2 is not essential for virus replication in tissue culture, and the human RSV leader region acts as a functional BRSV genome promoter. J. Virol. **73**:251–259.
10. **Carneiro FA, Bianconi ML, Weissmuller G, Stauffer F, Da Poian AT.** 2002. Membrane recognition by vesicular stomatitis virus involves enthalpy-driven protein-lipid interactions. J. Virol. **76**:3756–3764.
11. **Chandran K, Sullivan NJ, Felbor U, Whelan SP, Cunningham JM.** 2005. Endosomal proteolysis of the Ebola virus glycoprotein is necessary for infection. Science **308**:1643–1645.
12. **Cheng LW, et al.** 2005. Use of RNA interference in Drosophila S2 cells to identify host pathways controlling compartmentalization of an intracellular pathogen. Proc. Natl. Acad. Sci. U. S. A. **102**:13646–13651.
13. **Cherry S, et al.** 2006. COPI activity coupled with fatty acid biosynthesis is required for viral replication. PLoS Pathog. **2**:e102.
14. **Cureton DK, Massol RH, Saffarian S, Kirchhausen TL, Whelan SP.** 2009. Vesicular stomatitis virus enters cells through vesicles incompletely coated with clathrin that depend upon actin for internalization. PLoS Pathog. **5**:e1000394.
15. **Cureton DK, Massol RH, Whelan SP, Kirchhausen T.** 2010. The length of vesicular stomatitis virus particles dictates a need for actin assembly during clathrin-dependent endocytosis. PLoS Pathog. **6**:e1001127.
16. **Daro E, Sheff D, Gomez M, Kreis T, Mellman I.** 1997. Inhibition of endosome function in CHO cells bearing a temperature-sensitive defect in the coatomer (COPI) component epsilon-COP. J. Cell Biol. **139**: 1747–1759.
17. **Derre I, Pypaert M, Dautry-Varsat A, Agaisse H.** 2007. RNAi screen in Drosophila cells reveals the involvement of the Tom complex in Chlamydia infection. PLoS Pathog. **3**:1446–1458.
18. **Elwell CA, Ceesay A, Kim JH, Kalman D, Engel JN.** 2008. RNA interference screen identifies Abl kinase and PDGFR signaling in Chlamydia trachomatis entry. PLoS Pathog. **4**:e1000021.
19. **Gazina EV, Mackenzie JM, Gorrell RJ, Anderson DA.** 2002. Differential requirements for COPI coats in formation of replication complexes among three genera of Picornaviridae. J. Virol. **76**:11113–11122.
20. **Ghosh RN, Gelman DL, Maxfield FR.** 1994. Quantification of low density lipoprotein and transferrin endocytic sorting HEp2 cells using confocal microscopy. J. Cell Sci. **107**:2177–2189.
21. **Gu F, Aniento F, Parton RG, Gruenberg J.** 1997. Functional dissection of COP-I subunits in the biogenesis of multivesicular endosomes. J. Cell Biol. **139**:1183–1195.

22. **Gu F, Gruenberg J.** 2000. ARF1 regulates pH-dependent COP functions in the early endocytic pathway. J. Biol. Chem. **275**:8154–8160.
23. **Guo Q, Vasile E, Krieger M.** 1994. Disruptions in Golgi structure and membrane traffic in a conditional lethal mammalian cell mutant are corrected by epsilon-COP. J. Cell Biol. **125**:1213–1224.
24. **Hao L, et al.** 2008. Drosophila RNAi screen identifies host genes important for influenza virus replication. Nature **454**:890–893.
25. **Heinrich BS, Cureton DK, Rahmeh AA, Whelan SP.** 2010. Protein expression redirects vesicular stomatitis virus RNA synthesis to cytoplasmic inclusions. PLoS Pathog. **6**:e1000958.
26. **Helms JB, Rothman JE.** 1992. Inhibition by brefeldin A of a Golgi membrane enzyme that catalyses exchange of guanine nucleotide bound to ARF. Nature **360**:352–354.
27. **Hobbie L, Fisher AS, Lee S, Flint A, Krieger M.** 1994. Isolation of three classes of conditional lethal Chinese hamster ovary cell mutants with temperature-dependent defects in low density lipoprotein receptor stability and intracellular membrane transport. J. Biol. Chem. **269**: 20958–20970.
28. **Irurzun A, Perez L, Carrasco L.** 1993. Brefeldin A blocks protein glycosylation and RNA replication of vesicular stomatitis virus. FEBS Lett. **336**:496–500.
29. **Johannsdottir HK, Mancini R, Kartenbeck J, Amato L, Helenius A.** 2009. Host cell factors and functions involved in vesicular stomatitis virus entry. J. Virol. **83**:440–453.
30. **Jounai N, et al.** 2007. The Atg5 Atg12 conjugate associates with innate antiviral immune responses. Proc. Natl. Acad. Sci. U. S. A. **104**: 14050–14055.
31. **Karlas A, et al.** 2010. Genome-wide RNAi screen identifies human host factors crucial for influenza virus replication. Nature **463**:818–822.
32. **Le Blanc I, et al.** 2005. Endosome-to-cytosol transport of viral nucleocapsids. Nat. Cell Biol. **7**:653–664.
33. **Lee HK, Lund JM, Ramanathan B, Mizushima N, Iwasaki A.** 2007. Autophagy-dependent viral recognition by plasmacytoid dendritic cells. Science **315**:1398–1401.
34. **Lefrancios L, Lyles DS.** 1982. The interaction of antibody with the major surface glycoprotein of vesicular stomatitis virus. I. Analysis of neutralizing epitopes with monoclonal antibodies. Virology **121**:157–167.
35. **Li Q, et al.** 2009. A genome-wide genetic screen for host factors required for hepatitis C virus propagation. Proc. Natl. Acad. Sci. U. S. A. **106**: 16410–16415.
36. **Lippincott-Schwartz J, et al.** 1991. Brefeldin A's effects on endosomes, lysosomes, and the TGN suggest a general mechanism for regulating organelle structure and membrane traffic. Cell **67**:601–616.
37. **Lippincott-Schwartz J, Yuan LC, Bonifacino JS, Klausner RD.** 1989. Rapid redistribution of Golgi proteins into the ER in cells treated with brefeldin A: evidence for membrane cycling from Golgi to ER. Cell **56**: 801–813.
38. **Lozach PY, et al.** 2010. Entry of bunyaviruses into mammalian cells. Cell Host Microbe **7**:488–499.
39. **Lyles DS, Rupprecht CE.** 2007. *Rhabdoviridae*, p 1363–1408. *In*Knipe DM, Howley PM, Griffin DE, Lamb RA, Martin MA, Roizman B, Straus SE (ed), Fields virology, 5th ed. Lippincott Williams & Wilkins, Hagerstown, MD.
40. **Makarow M, Nevalainen LT, Kaariainen L.** 1986. Expression of the RNA genome of an animal virus in Saccharomyces cerevisiae. Proc. Natl. Acad. Sci. U. S. A. **83**:8117–8121.
41. **Matlin KS, Reggio H, Helenius A, Simons K.** 1982. Pathway of vesicular stomatitis virus entry leading to infection. J. Mol. Biol. **156**:609–631.
42. **Miller DK, Lenard J.** 1980. Inhibition of vesicular stomatitis virus infection by spike glycoprotein. Evidence for an intracellular, G protein-requiring step. J. Cell Biol. **84**:430–437.
43. **Mire CE, Dube D, Delos SE, White JM, Whitt MA.** 2009. Glycoprotein-dependent acidification of vesicular stomatitis virus enhances release of matrix protein. J. Virol. **83**:12139–12150.
44. **Mire CE, White JM, Whitt MA.** 2010. A spatio-temporal analysis of matrix protein and nucleocapsid trafficking during vesicular stomatitis virus uncoating. PLoS Pathog. **6**:e1000994.
45. **Misselwitz B, et al.** 2011. RNAi screen of Salmonella invasion shows role of COPI in membrane targeting of cholesterol and Cdc42. Mol. Syst. Biol. **7**:474.
46. **Misumi Y, et al.** 1986. Novel blockade by brefeldin A of intracellular transport of secretory proteins in cultured rat hepatocytes. J. Biol. Chem. **261**:11398–11403.
47. **Mudd JA, Leavitt RW, Kingsbury DT, Holland JJ.** 1973. Natural selection of mutants of vesicular stomatitis virus by cultured cells of Drosophila melanogaster. J. Gen. Virol. **20**:341–351.
48. **Newcomb WW, Brown JC.** 1981. Role of the vesicular stomatitis virus matrix protein in maintaining the viral nucleocapsid in the condensed form found in native virions. J. Virol. **39**:295–299.
49. **Peng G, et al.** 2010. Cryo-EM model of the bullet-shaped vesicular stomatitis virus. Science **327**:689–693.
50. **Philips JA, Rubin EJ, Perrimon N.** 2005. Drosophila RNAi screen reveals CD36 family member required for mycobacterial infection. Science **309**: 1251–1253.
51. **Ramet M, Manfruelli P, Pearson A, Mathey-Prevot B, Ezekowitz RA.** 2002. Functional genomic analysis of phagocytosis and identification of a Drosophila receptor for E. coli. Nature **416**:644–648.
52. **Razi M, Chan EY, Tooze SA.** 2009. Early endosomes and endosomal coatomer are required for autophagy. J. Cell Biol. **185**:305–321.
53. **Rigaut KD, Birk DE, Lenard J.** 1991. Intracellular distribution of input vesicular stomatitis virus proteins after uncoating. J. Virol. **65**:2622–2628.
54. **Robineau S, Chabre M, Antonny B.** 2000. Binding site of brefeldin A at the interface between the small G protein ADP-ribosylation factor 1 (ARF1) and the nucleotide-exchange factor Sec7 domain. Proc. Natl. Acad. Sci. U. S. A. **97**:9913–9918.
55. **Schott DH, Cureton DK, Whelan SP, Hunter CP.** 2005. An antiviral role for the RNA interference machinery in Caenorhabditis elegans. Proc. Natl. Acad. Sci. U. S. A. **102**:18420–18424.
56. **Shelly S, Lukinova N, Bambina S, Berman A, Cherry S.** 2009. Autophagy is an essential component of Drosophila immunity against vesicular stomatitis virus. Immunity **30**:588–598.
57. **Sieczkarski SB, Whittaker GR.** 2003. Differential requirements of Rab5 and Rab7 for endocytosis of influenza and other enveloped viruses. Traffic **4**:333–343.
58. **Sun X, Yau VK, Briggs BJ, Whittaker GR.** 2005. Role of clathrin-mediated endocytosis during vesicular stomatitis virus entry into host cells. Virology **338**:53–60.
59. **Szilagyi JF, Uryvayev L.** 1973. Isolation of an infectious ribonucleoprotein from vesicular stomatitis virus containing an active RNA transcriptase. J. Virol. **11**:279–286.
60. **Tai AW, et al.** 2009. A functional genomic screen identifies cellular cofactors of hepatitis C virus replication. Cell Host Microbe **5**:298–307.
61. **Thomas D, et al.** 1985. Mass and molecular composition of vesicular stomatitis virus: a scanning transmission electron microscopy analysis. J. Virol. **54**:598–607.
62. **Vandepol SB, Lefrancois L, Holland JJ.** 1986. Sequences of the major antibody binding epitopes of the Indiana serotype of vesicular stomatitis virus. Virology **148**:312–325.
63. **Verheije MH, et al.** 2008. Mouse hepatitis coronavirus RNA replication depends on GBF1-mediated ARF1 activation. PLoS Pathog. **4**:e1000088.
64. **Whealy ME, Card JP, Meade RP, Robbins AK, Enquist LW.** 1991. Effect of brefeldin A on alphaherpesvirus membrane protein glycosylation and virus egress. J. Virol. **65**:1066–1081.
65. **Whelan SP, Ball LA, Barr JN, Wertz GT.** 1995. Efficient recovery of infectious vesicular stomatitis virus entirely from cDNA clones. Proc. Natl. Acad. Sci. U. S. A. **92**:8388–8392.
66. **Whelan SP, Wertz GW.** 2002. Transcription and replication initiate at separate sites on the vesicular stomatitis virus genome. Proc. Natl. Acad. Sci. U. S. A. **99**:9178–9183.
67. **White J, Matlin K, Helenius A.** 1981. Cell fusion by Semliki Forest, influenza, and vesicular stomatitis viruses. J. Cell Biol. **89**:674–679.
68. **Whitney JA, Gomez M, Sheff D, Kreis TE, Mellman I.** 1995. Cytoplasmic coat proteins involved in endosome function. Cell **83**:703–713.
69. **Wilkins C, et al.** 2005. RNA interference is an antiviral defence mechanism in Caenorhabditis elegans. Nature **436**:1044–1047.